

# Unravelling the Origins of Contact Recombination for Localized Laser-Doped Contacts

Marco Ernst<sup>1</sup>, Jonas D. Huyeng<sup>1,2</sup>, Daniel Walter<sup>1</sup>, Kean Chern Fong<sup>1</sup> and Andrew Blakers<sup>1</sup>

<sup>1</sup>Centre for Sustainable Energy Systems, Australian National University, Canberra, ACT 2600, Australia

<sup>2</sup>Fraunhofer Institute for Solar Energy Systems (ISE), Heidenhofstrasse 2, 79110 Freiburg, Germany

**Abstract** — Both localized laser-doping and contact opening are utilized in fabrication of high-efficiency solar cell devices. In this work, we present an experimental method to separate the origins of the lumped recombination parameter for localized contacts. We attribute the main source of recombination after laser doping to small edges around the laser-processed regions ( $j_{0,e} \approx 10,000 \text{ fA/cm}^2$ ), while the center areas have a non-negligible contribution ( $j_{0,a} \approx 2,000\text{-}3,000 \text{ fA/cm}^2$ ). Both contributions can be significantly reduced by annealing. At the same time, the non-optimized laser process achieves contact resistivity values as low as  $70 \mu\Omega \text{ cm}^2$ .

**Index Terms** — Recombination, laser doping, laser ablation, edge recombination, silicon.

## I. INTRODUCTION

Highly precise laser processes such as laser doping (LD) and laser contact opening (LCO) are widely adopted in solar cell devices to form localized contacts whilst minimizing thermal budget. LD processes are used in selective emitter structures [1-3] and for creating localized contacts in high-efficiency concepts [4-6].

However, it is known that LD can cause dislocations in the heavily doped layers, which can adversely affect the recombination at contacts and as a result final cell performance [7-9].

Laser-induced dislocations at the edges of localized LD areas have been identified as a key contributor to the recombination of LD contacts [10, 11]. Lumped recombination parameter values of metallized localized contacts have been determined through photoluminescence (PL) methods [12, 13] and dynamic infrared lifetime mapping [14].

In this work, we present a method to separate the contributions of edge and area regions to the commonly measured lumped recombination parameter by systematically varying size and edge to area ratio of fabricated local contacts and combining results with numerical simulations.

## II. EXPERIMENTAL

We use  $1000 \Omega \text{ cm}$ , n-type float zone, 100 mm silicon wafers with a thickness of  $396 \mu\text{m}$ . All wafers undergo a Tabula Rasa treatment at  $1000^\circ\text{C}$  in an oxygen atmosphere before further processing, to minimize wafer induced effects.

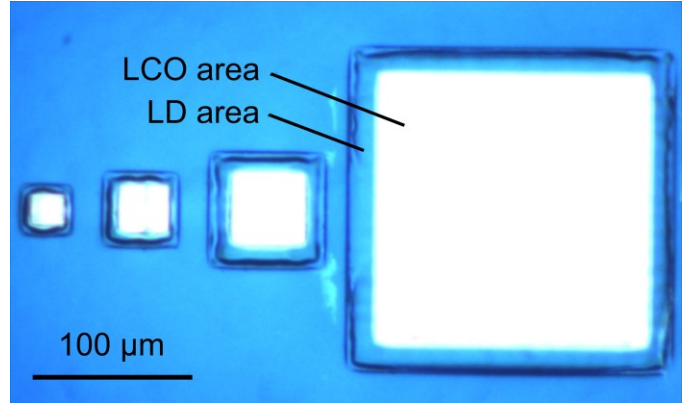


Fig. 1. Microscope image illustrating the variation of laser-doping size after laser-contact opening confined to a region smaller than the laser-doped areas.

After removal of  $\text{SiO}_2$  and RCA standard clean, we grow a phosphorus-doped silica glass (PSG) layer in a thermal batch process at  $750^\circ\text{C}$ , by oxidation in a  $\text{POCl}_3\text{:N}_2\text{:O}_2$  atmosphere. This PSG deposition process creates a light background diffusion in the unprocessed areas of the wafer.

Directly after PSG deposition, we use an Excimer laser source that emits light at a wavelength of  $248 \text{ nm}$  and a pulse width of  $25 \text{ ns}$  to perform single-pulse laser doping (LD) of the substrates. We vary laser fluence  $\phi$ , LD spot pitch, and LD spot size  $s$  with a variable aperture mask of the flat-top laser beam. After cleaning, we anneal the wafers in a batch process under oxygen atmosphere at  $700^\circ\text{C}$  for 15 min, which creates a very thin  $\text{SiO}_2$  layer, comparable to a native oxide. For passivating the surface, we then deposit an  $88 \text{ nm}$   $\text{Si}_3\text{N}_4$  layer on all sides by means of low pressure chemical vapor deposition (LPCVD) at  $745^\circ\text{C}$ .

Subsequently, we perform local laser contact opening (LCO) on the dielectric stack, which was previously optimized to prevent laser damage from the LCO process. We use the same Excimer laser setup as for LD and carefully align the two laser processes using alignment marks on the wafer. Figure 1 shows a microscope image of the variation in laser-spot size after contact opening on a test pattern fabricated on each wafer. The bright LCO regions extend to an area slightly smaller than the laser-doped areas thus covering the edges of the LD areas.

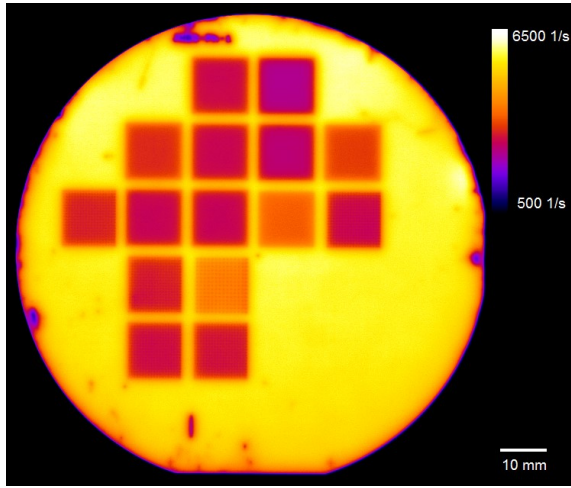


Fig. 2. PL image of local laser-doped contacts. The different processed square-shaped areas feature different laser spot sizes, pitches and laser fluences. The bottom right quarter (not laser processed) is used for QSSPC reference measurements to fit numerical simulation.

Finally, we evaporate a layer of aluminium to form the electrodes and metal-semiconductor contacts in LCO areas.

Please note that the PSG layer deposition conditions and passivating dielectric stack have not been optimized for this study. However, we varied a number of laser doping parameters and demonstrated our method as shown below.

#### A. Recombination samples

We fabricate two sets of recombination samples and vary laser fluence  $\phi = 1.3 \text{ J/cm}^2$  and  $2.1 \text{ J/cm}^2$  in both cases.

In the first set we prepare  $12 \text{ mm} \times 12 \text{ mm}$ -sized large-area laser-doped regions by stitching square LD spots with a spot size  $s = 500 \mu\text{m}$ . From these large-area doped samples we measure sheet resistance  $R_{\text{sheet}}$  by four-point probe (4pp) and doping profile  $n(z)$  via electrochemical C-V measurements (ECV). We correct the dopant profiles using the actual etched area determined from optical microscope images.

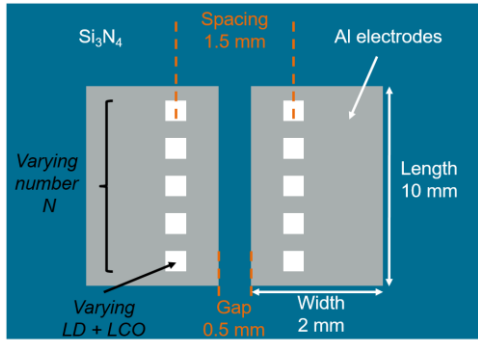


Fig. 3. Illustration of test structure to determine local contact resistivity. Numbers and sizes of local contacts (white) are varied and total resistance between two pads is measured.

We also measure the photoluminescence signal of the laser-doped regions and determine the recombination parameter  $j_{0,\text{LD}}$  by calibrating the measured PL signal of an unprocessed reference region to a quasi-steady state photoconductance (QSSPC) measurement of the same region [13].

In the second set we fabricate samples with localized laser-doped contacts. On these samples we vary the laser spot sizes between  $s = 30 \mu\text{m}$  and  $s = 210 \mu\text{m}$  for the same laser fluences as for the large-area LD samples. The localized laser-doped regions are arranged in regular arrays with varied pitch to achieve LD area coverage between 7 and 27%.

We measure the PL signal of the samples after laser doping. An image of one of these wafers is shown in Fig. 2. By means of three-dimensional numerical simulation we extract the lumped recombination parameter  $j_{0,\text{ave}}$  of the localized laser-doped contact regions with varying contact size, pitch and laser fluence.

#### B. Contact resistance samples

For the determination of contact resistivity, we use  $1.4 \Omega \text{ cm}$ , Cz-Si wafers with a thickness of  $300 \mu\text{m}$  and prepare a structure with localized laser-doped contacts. We select the same polarity for wafer base doping and local contacts, so that the structure is purely ohmic (*cf.* [15]).

We vary the number of spots  $N$ , spot size  $s$  (Fig. 1) and laser doping fluence  $\phi$  and align the local contacts collinear and equidistant under pairs of Al-electrodes with a distance of  $1.5 \text{ mm}$  between the two contact rows, as sketched in Fig. 3.

We measure the total resistance between two contact pads after a forming gas anneal (FGA) at  $300^\circ\text{C}$  to improve contact quality. We use Quokka 3 [16] to simulate the structure for different numbers of local contacts  $N$  and fit the total resistance to determine the contact resistivity  $\rho_C$ . The analysis procedure is described in detail in Ref. [17].

## III. RESULTS

Table I lists the measured sheet resistance  $R_{\text{sheet}}$  of an unprocessed reference region and large-area laser-doped regions for the two laser fluences  $\phi = 1.3 \text{ J/cm}^2$  and  $2.1 \text{ J/cm}^2$  fabricated from a single pulse process. The contact resistance values determined in Ref. [17] for localized contacts are also listed in Table I.

TABLE I  
PARAMETERS DERIVED FOR PHOSPHORUS LASER DOPING

$\phi$ ( $\text{J/cm}^2$ )	$R_{\text{sheet}}$ ( $\Omega/\square$ )	$j_{0,\text{LD}}$ ( $\text{fA/cm}^2$ )	$\rho_C^*$ $\text{m}\Omega \text{ cm}^2$
1.3	$186 \pm 20$	$3,970 \pm 400$	0.35
2.1	$60 \pm 7$	$3,100 \pm 310$	0.07
REF**	$> 1,000$	$180 \pm 10$	-

\*After FGA at  $300^\circ\text{C}$ ; \*\*Unprocessed reference area.

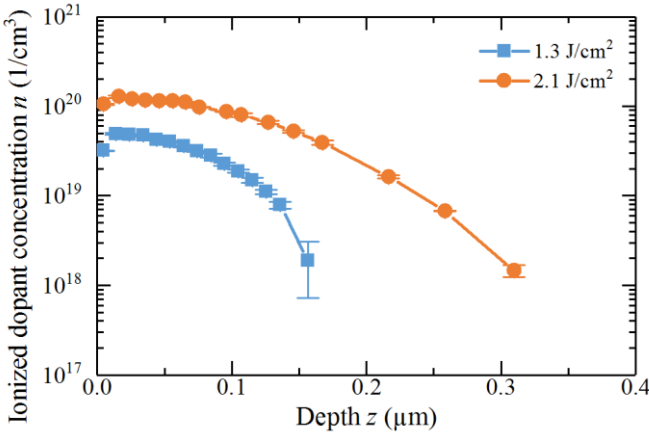


Fig. 4. Charge carrier concentration as measured by ECV for phosphorus laser doping (solid) for two different fluences. The higher fluence results in a higher surface concentration and a deeper profile.

The light phosphorus background diffusion from the PSG deposition process yields a surface recombination parameter of  $180 \pm 10 \text{ fA/cm}^2$  in the unprocessed regions of the wafer, without any passivating dielectric films. This value is used to calibrate the PL measurement. The extracted recombination parameter  $j_{0,\text{LD}}$  for the large area LD are listed in Table I, for the identical process state. The doping profiles for these parameters are shown in Fig. 4.

We measure the PL signal on the samples with localized laser-doped contacts. The simulated PL signal is calibrated to the measurements by PL measurements of an unprocessed reference region and quasi-steady state photoconductance (QSSPC) measurement of the same region. This procedure yields the surface and bulk properties in the unprocessed reference region of the wafer. The internal and external optical properties of the samples are modelled using OPAL 2 [18].

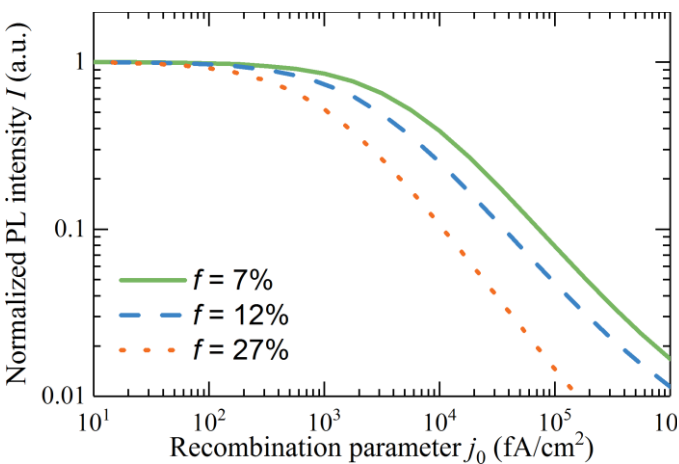


Fig. 5. Example for the determination of  $j_0$  from numerical simulation of PL intensity for three area fractions  $f$ . As can be seen, for low local recombination parameters  $j_0$  the sensitivity of the method is limited, as bulk lifetime limits the measurable PL intensity.

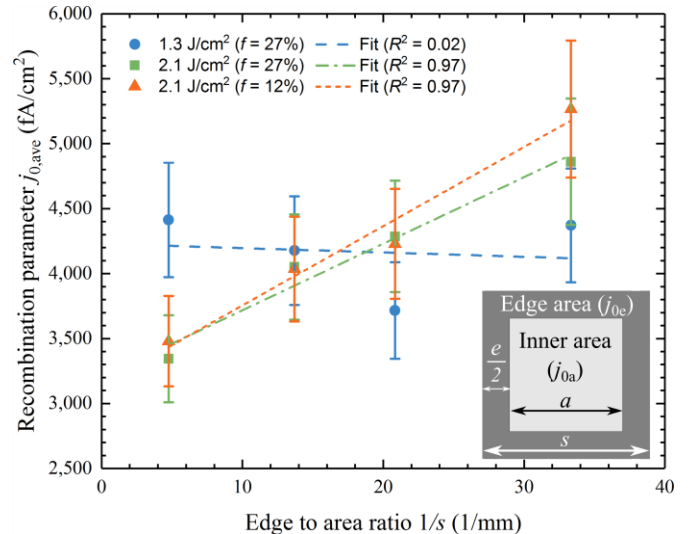


Fig. 6. Measured lumped recombination parameter  $j_{0,\text{ave}}$  as a function of edge to area ratio  $1/s$ , for localized contacts from PSG laser-doping. For the blue (dashed) line, there is no significant dependency, whereas the orange (short dashed) and green (dash-dotted) lines show a clear linear trend. Inset: Geometrical description of square laser spots with small edge area.

To extract the lumped recombination parameter  $j_{0,\text{ave}}$  of the localized laser-doped regions we simulate the PL intensity with Quokka 2 for each coverage fraction  $f$  (Fig. 5). In the three-dimensional numerical simulations we sweep  $j_{0,\text{ave}}$  while assuming identical properties of the unprocessed regions between the laser spots ( $1-f$ ) as determined in the reference region. To determine a meaningful average, we only evaluate the signal well inside the laser processed square. We then compare the measured PL intensity in the laser processed areas (Fig. 2) to calculate  $j_{0,\text{ave}}$  [13].

We separate the edge contribution ( $j_{0,e}$ ) from the laser-doped center area ( $j_{0,a}$ ) of localized LD contact regions by varying the size of the laser spot  $s$ . In order to keep the doped area fraction  $f = (s^2/p^2)$  constant for different spot sizes, we adjust the pitch  $p$  between spots. In this way, only the edge to area ratio ( $1/s$ ) of our laser spots is varied.

In Figure 6 we plot  $j_{0,\text{ave}}$  against  $1/s$  for three out of six parameter variations. The results of all parameters are listed in Table II.

TABLE II  
LOCALIZED CONTACT RECOMBINATION PARAMETERS  
DERIVED FOR PHOSPHORUS LASER DOPING

$\phi$ (J/cm²)	$f$ (%)	$j_{0,a}$ (fA/cm²)	$k$ (fA/cm² mm)	$j_{0,e}^*$ (fA/cm²)
1.3	12	3,340**	-	-
1.3	27	4,170**	-	-
2.1	7	2,285 ± 115	72.7 ± 5.5	9,550 ± 4,480
2.1	12	2,658 ± 182	55.1 ± 8.7	11,370 ± 5,130
2.1	12	3,206 ± 132	51.2 ± 6.3	9,610 ± 4,600
2.1	27	3,145 ± 155	61.0 ± 7.4	10,770 ± 5,030

\*Assuming edge width  $e = 4 \pm 2 \mu\text{m}$ ; \*\*Mean value of  $j_{0,\text{ave}}$

In the inset of Fig. 6 we describe the laser spot by three different geometrical parameters: spot size  $s$ , inner area length  $a$  and edge width  $e \equiv s - a$ . Note that the edge length  $e$  is the total width of both edges. Assuming an area-proportional contribution of  $j_{0,a}$  and  $j_{0,e}$  we weight them with  $a^2/s^2$  and  $(s^2 - a^2)/s^2$ , respectively, to describe the extracted average recombination parameter as:

$$j_{0,\text{ave}} = j_{0,a} + 2e\Delta j_0 \frac{s}{s^2} - \Delta j_0 e^2 \frac{1}{s^2}, \quad (1)$$

where  $\Delta j_0 := (j_{0,e} - j_{0,a})$ . For  $e \ll s$  we can approximate  $j_{0,\text{ave}}$  with:

$$j_{0,\text{ave}} \approx j_{0,a} + 2e(j_{0,e} - j_{0,a}) \frac{1}{S}. \quad (2)$$

We fit Eq. (2) to our measurements and extract the fit parameters  $j_{0,a}$  and  $k \equiv 2e(j_{0,e} - j_{0,a})$ . For the low laser fluence  $\phi = 1.3 \text{ J/cm}^2$ , we observe no correlation of  $j_{0,\text{ave}}$  with  $1/s$ , thus implying negligible edge contributions. For the higher laser fluence  $\phi = 2.1 \text{ J/cm}^2$ , we find a clear linear correlation of  $j_{0,\text{ave}}$  with  $1/s$ . Edge recombination clearly has a strong contribution to the lumped recombination parameter  $j_{0,\text{ave}}$  and the edge region is much smaller than the laser spot size.

Due to the ambiguity of the linear approximation, at this stage we can only give the implicit relation

$$j_{0,e} \equiv j_{0,e}(e) = j_{0,a} + \frac{k}{2e}. \quad (3)$$

In Table II we list the fit parameters  $j_{0,a}$  and  $k$  and their respective standard fitting error for all samples investigated. The edge recombination is calculated using Eq. (3) assuming an edge width of  $e = 4 \pm 2 \mu\text{m}$ . The edge recombination parameter  $j_{0,e}$  exceeds the recombination parameter of the laser-doped center area  $j_{0,a}$  by a factor greater than 3 to 4.

In case of the fluence  $\phi = 1.3 \text{ J/cm}^2$  the fit did not result in a significant dependence on the edge to area ratio and thus no fit parameters were determined. Instead, the mean value for  $j_{0,\text{ave}}$  is given in place of  $j_{0,a}$ . These values agree within the range of uncertainty with the values determined from large-area doping at the same fluence.

Lumped recombination parameters have also been determined after surface passivation with LPCVD  $\text{Si}_3\text{N}_4$ . However, the bulk lifetime degraded during this process thus reducing the sensitivity of the method. An optimized low-temperature passivation process could be used to prevent this.

Nevertheless, after passivation of the samples the measured PL intensities in the laser-processed regions even exceeds the PL intensity of the reference regions and thus indicates a successful curing of the laser-induced damage. As can be seen from Fig. 5, in such a case only an upper limit for the local recombination parameter can be given, due to the low sensitivity of the PL method for recombination values below approximately  $300 - 1,000 \text{ fA/cm}^2$ .

## V. CONCLUSION

In this paper we described a method to determine the contributions of edge and area regions to the lumped recombination parameter of local contacts. We successfully applied this method to fabricated locally laser-doped contacts.

We could show that for our sample system higher laser fluence in laser doping introduces a dominant recombination at the laser spot edges ( $j_{0,e} \approx 10,000 \text{ fA/cm}^2$ ), which can be successfully cured.

Further understanding, verification and optimization of used processes are our targets for future work, *e.g.* by micro PL spectroscopy ( $\mu$ PLS) analysis to spatially resolve the structure of local contacts and damaged regions.

## ACKNOWLEDGEMENT

This Program has been supported by the Australian Government through the Australian Renewable Energy Agency (ARENA). Responsibility for the views, information or advice expressed herein is not accepted by the Australian Government.

J.D. Huyeng acknowledges funding by the center of renewable energy of the University of Freiburg, within the interdisciplinary graduate school “DENE”.

## REFERENCES

- [1] U. Besu-Vetrella, L. Pirozzi, E. Salza, G. Ginocchietti, F. Ferrazza, L. Ventura, A. Slaoui, and J. C. Muller, “Large area, screen printed silicon solar cells with selective emitter made by laser overdoping and RTA spin-on glasses,” in *26th IEEE Photovoltaic Specialists Conference*, 1997, pp. 135–138.
- [2] U. Jäger, M. Okanovic, M. Hörtelis, A. Grohe, and R. Preu, “Selective Emitter by Laser Doping from Phosphosilicate Glass,” in *24th European Photovoltaic Solar Energy Conference and Exhibition*, 2009, 2CV.5.9, pp. 1740–1743.
- [3] T. Röder, P. Grabitz, S. Eisele, C. Wagner, J. R. Kohler, and J. H. Werner, “0.4% absolute efficiency gain of industrial solar cells by laser doped selective emitter,” in *34th IEEE Photovoltaic Specialists Conference*, 2009, pp. 000871–000873.
- [4] M. Dahlinger, B. Bazer-Bachi, T. C. Röder, J. R. Köhler, R. Zapf-Gottwick, and J. H. Werner, “22.0% Efficient Laser Doped back Contact Solar Cells,” *Energy Procedia*, vol. 38, pp. 250–253, 2013.
- [5] S. Singh, B. O’Sullivan, Récaman-Payo M., Uruena de Castro, A., M. Debucquoy, J. Szlufcik, and J. Poortmans, “Process Development on Photolithography Free IBC Solar Cells,” in *29th European PV Solar Energy Conference and Exhibition*, 2014, 2EO.1.2, pp. 672–675.
- [6] M. Ernst, E. Franklin, A. Fell, K. Fong, D. Walter, E.-C. Wang, T. Kho, and A. Blakers, “Fabrication of a 22.8% Efficient Back Contact Solar Cell With Localized Laser-Doping,” *physica status solidi (a)*, vol. 31, p. 1700318, 2017.
- [7] A. Sugianto, B. S. Tjahjono, J. H. Guo, and S. R. Wenham, “Impact of laser induced defects on the performance of solar cells using localised laser doped regions beneath the metal contacts,” in *22nd European Photovoltaic Solar Energy Conference*, 2007, pp. 1759–1762.
- [8] Z. Hameiri, T. Puzzer, L. Mai, A. B. Sproul, and S. R. Wenham, “Laser induced defects in laser doped solar cells,” *Progress in*

- Photovoltaics: Research and Applications*, vol. 19 (4), pp. 391–405, 2011.
- [9] L. Xu, K. Weber, A. Fell, Z. Hameiri, S. P. Phang, X. Yang, and E. Franklin, “The Impact of SiO<sub>2</sub>/SiNx Stack Thickness on Laser Doping of Silicon Solar Cell,” *IEEE Journal of Photovoltaics*, vol. 4 (2), pp. 594–600, 2014.
  - [10] H. T. Nguyen, Y. Han, M. Ernst, A. Fell, E. Franklin, and D. Macdonald, “Dislocations in laser-doped silicon detected by micro-photoluminescence spectroscopy,” *Applied Physics Letters*, vol. 107 (2), p. 022101, 2015.
  - [11] Y.-J. Han, E. Franklin, A. Fell, M. Ernst, H. T. Nguyen, and D. Macdonald, “Low-temperature micro-photoluminescence spectroscopy on laser-doped silicon with different surface conditions,” *Applied Physics A*, vol. 122 (4), 2016.
  - [12] V. Shanmugam, T. Mueller, A. G. Aberle, and J. Wong, “Determination of metal contact recombination parameters for silicon wafer solar cells by photoluminescence imaging,” *Solar Energy*, vol. 118, pp. 20–27, 2015.
  - [13] M. Ernst, A. Fell, E. Franklin, and K. J. Weber, “Characterization of Recombination Properties and Contact Resistivity of Laser-Processed Localized Contacts From Doped Silicon Nanoparticle Ink and Spin-On Dopants,” *IEEE Journal of Photovoltaics*, vol. 7 (2), pp. 471–478, 2017.
  - [14] J. Mueller, K. Bothe, S. Gatz, F. Haase, C. Mader, and R. Brendel, “Recombination at laser-processed local base contacts by dynamic infrared lifetime mapping,” *Journal of Applied Physics*, vol. 108 (12), p. 124513, 2010.
  - [15] A. Fell, S. Surve, E. Franklin, and K. J. Weber, “Characterization of Laser-Doped Localized p-n Junctions for High Efficiency Silicon Solar Cells,” *IEEE Transactions on Electron Devices*, vol. 61 (6), pp. 1943–1949, 2014.
  - [16] A. Fell, J. Schön, M. C. Schubert, S. W. Glunz, “The concept of skins for silicon solar cell modeling,” *Solar Energy Materials and Solar Cells*, vol. 173, pp. 128–133, 2017.
  - [17] J. Huyeng, M. Ernst, K. Fong, D. Walter, A. Blakers, “Implications of laser-doping parameters and contact opening size on contact resistivity,” in *7<sup>th</sup> World Conference on Photovoltaic Energy Conversion*, this conference, 2018.
  - [18] K. R. McIntosh and S. C. Baker-Finch, “OPAL 2: Rapid optical simulation of silicon solar cells,” in *38<sup>th</sup> IEEE Photovoltaic Specialists Conference*, 2012, pp. 265–271.